buildings

MDPI

Review

Thermochromic Oxide-Based Thin Films and Nanoparticle Composites for Energy-Efficient Glazings

Claes G. Granqvist * and Gunnar A. Niklasson

Department of Engineering Sciences, The Ångström Laboratory, Uppsala University, P.O. Box 534, SE-75121 Uppsala, Sweden; Gunnar.Niklasson@Angstrom.uu.se

* Correspondence: claes-goran.granqvist@angstrom.uu.se; Tel.: +46-18-471-3067

Academic Editor: Cinzia Buratti

Received: 24 November 2016; Accepted: 20 December 2016; Published: 29 December 2016

Abstract: Today's advances in materials science and technology can lead to better buildings with improved energy efficiency and indoor conditions. Particular attention should be directed towards windows and glass facades—jointly known as "glazings"—since current practices often lead to huge energy expenditures related to excessive inflow or outflow of energy which need to be balanced by energy-intensive cooling or heating. This review article outlines recent progress in thermochromics, i.e., it deals with materials whose optical properties are strongly dependent on temperature. In particular, we discuss oxide-based thin surface coatings (thin films) and nanoparticle composites which can be deposited onto glass and are able to regulate the throughput of solar energy while the luminous (visible) properties remain more or less unaltered. Another implementation embodies lamination materials incorporating thermochromic (TC) nanoparticles. The thin films and nanocomposites are based on vanadium dioxide (VO_2), which is able to change its properties within a narrow temperature range in the vicinity of room temperature and either reflects or absorbs infrared light at elevated temperatures, whereas the reflectance or absorptance is much smaller at lower temperatures. The review outlines the state of the art for these thin films and nanocomposites with particular attention to recent developments that have taken place in laboratories worldwide. Specifically, we first set the scene by discussing environmental challenges and their relationship with TC glazings. Then enters VO_2 and we present its key properties in thin-film form and as nanoparticles. The next part of the article gives perspectives on the manufacturing of these films and particles. We point out that the properties of pure VO_2 may not be fully adequate for buildings and we elaborate how additives, antireflection layers, nanostructuring and protective over-coatings can be employed to yield improved performance and durability that make TC glazings of considerable interest for building-related applications. Finally, we briefly describe recent developments towards TC light scattering and draw some final conclusions.

Keywords: thermochromism; coating; thin film; nanoparticle; vanadium dioxide; energy-efficient glazing; sputter deposition

1. Introduction

The current energy–environment nexus, and the challenges it imposes on society, serves as a driving force behind many endeavours in research and development. At the basis of these challenges lies the fact that the measured concentration of carbon dioxide in the Earth's atmosphere is rising dramatically; it was ~315 ppm at the end of the 1950s and now regularly exceeds ~400 ppm [1]. Furthermore, the rate of increase has almost tripled during this time span. The increased amount of CO_2 has its origin in energy generation—specifically unrestrained burning of coal, oil and gas—and is

widely believed to lead to global warming and rising sea levels [2]. There may also be many secondary harmful impacts of climate change related to, for example, socioeconomic effects and increased risk for human conflict [3–5].

Furthermore, the world's population is growing rapidly both in absolute and relative numbers and is predicted to be 50% larger by the year 2100 than it is today [6]. This population is increasingly agglomerated in urban centres, and it is expected that 70% of all people will be living in such areas by the year 2050 [7]. The centres behave as "urban heat islands" and may reach temperatures that can be several degrees in excess of those in the surrounding countryside [8]. Hence, the "urban heat island" effect exacerbates CO_2-induced climate change [9] for the majority of the world's population. The effects of human activities are already pervasive enough that the current geological era—i.e., the Anthropocene—is considered distinctly different from the period prior to the Industrial Revolution, known as the Holocene [10].

It is evident that the global energy sector must be decarbonized, and this realization points sharply to the importance of improving buildings which are responsible for 30%–40% of the worldwide use of primary energy [11]. In fact, the impact of buildings is presently increasing in many parts of the world, and their part of the energy use in the USA, for example, was 34% in 1980 and as large as 41% in 2010 [12], and nothing indicates that this trend is changing. Another reason to consider buildings ensues from the fact that, in industrialized countries, people spend as much as 80%–90% of their time indoors [13].

Energy efficiency in the built environment is too often disregarded as an opportunity for CO_2 abatement [14]. However, there are many "green" technologies, often with nano-attributes, that can be harnessed [15–23], and energy-efficient glazings—i.e., windows and glass facades—are one of the most important options. Today's glazings frequently permit excessive energy flows to enter or exit a building, which then necessitates energy-wasteful cooling or heating. One principle solution to this conundrum is to make the glazings small, but this is not acceptable in practice since precious indoors–outdoors contact and daylighting are then curtailed, and both of these features are essential for human well-being and task performance [24–26]. However, energy efficiency can be achieved with glazings permitting variable amounts of solar energy and visible light to be transmitted. These glazings are often referred to as "intelligent" or "smart" and are based on stimulus-responsive "chromogenic" materials [27,28].

This review article deals with thermochromic (TC) materials, which are characterized by temperature-dependent properties. Thin films of oxide-based materials of this type can let through more solar energy at low temperatures than at high temperatures, which means that energy-efficient glazings can introduce solar energy primarily when it is needed. TC-based fenestration was suggested already some three decades ago [29,30] but has not yet made it to the marketplace in the case of oxide-based materials for reasons that are discussed below. However, there have been a number of recent advances in thermochromics that indicate that practical implementation is feasible in buildings [31–40].

It is important to realize already from the outset that TC devices for buildings must be compatible with truly large-scale manufacturing. In order to get a feel for the magnitude, one should contemplate that flat-glass production—mostly by the float process—has been predicted to be 9.2×10^9 square meters per year in 2016 [41]. Having TC-based functionality on only a small fraction of the glazings of the world requires production units capable of handling square-kilometer-sized areas per year.

TC materials and devices need to be characterized with regard to their ability to transmit and reflect luminous (i.e., visible) and solar radiation. These properties are conveniently introduced by considering a number of spectra illustrated in Figure 1. Thermal radiation, as shown in Figure 1a, is governed by blackbody curves—which are shown for four values of the temperature τ—multiplied by a materials-specific emittance which is less than unity; it is apparent that this radiation lies at $\lambda > 2$ μm for normal ambient temperatures, where λ is wavelength. Solar radiation impinging upon the Earth's atmospheric envelope can be approximated by blackbody-like radiation pertaining to

the sun's surface temperature (5505 °C) and falls at $0.2 < \lambda < 3$ μm. At ground level and for typical clear-weather conditions, this radiation is representatively the one illustrated in Figure 1b, where the sharp minima are a consequence of molecular absorption in the air. Luminous radiation, finally, is represented by the bell-shaped curve in Figure 1b which extends over the $0.4 < \lambda < 0.7$ μm range and has a peak at 0.55 μm. Quantitative information for luminous (lum) and solar (sol) transmittance, indicated as $T_{\mathrm{lum}}(\tau)$ and $T_{\mathrm{sol}}(\tau)$, respectively, are obtained from

$$T_{\mathrm{lum,sol}}(\tau) = \int d\lambda\ \varphi_{\mathrm{lum,sol}}(\lambda)\ T(\lambda,\tau) / \int d\lambda\ \varphi_{\mathrm{lum,sol}}(\lambda), \tag{1}$$

where $T(\lambda,\tau)$ is temperature-dependent spectral transmittance, φ_{lum} is the spectral sensitivity of the human eye [42], and φ_{sol} denotes the "air mass 1.5" solar irradiance spectrum (for the sun at 37° above the horizon) [43]. Analogous formulas apply to reflectance R.

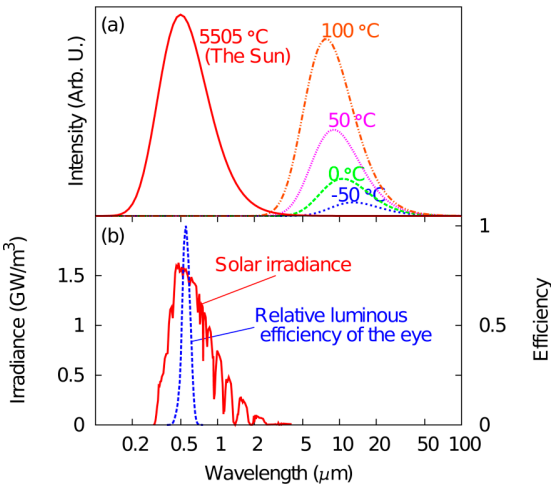

Figure 1. (**a**) Blackbody spectra for the indicated temperatures, which include the sun's surface temperature (the vertical scales differ for the spectra); (**b**) Typical solar irradiance spectrum for clear weather, and relative spectral sensitivity of the light-adapted human eye [33].

The TC materials are predominantly modulating the solar energy throughput, whereas the luminous performance is more or less temperature-independent, which implies that the modulation is conveniently characterized by

$$\Delta T_{\mathrm{sol}} \equiv T_{\mathrm{sol}}(\tau < \tau_c) - T_{\mathrm{sol}}(\tau > \tau_c), \tag{2}$$

where τ_c indicates the "critical" temperature at which the temperature-dependent properties are changed.

There are many reviews of TC materials and devices. The present one serves as an update and extension of some recent articles [40,44–46].

2. Basic Properties of Vanadium Dioxide Thin Films and Nanoparticles

There are many inorganic and organic thermochromic materials, but there is a limited number of possibilities for glazings, especially if the focus is on oxide-based thin films and nanoparticle composites suitable for large-area applications. Figure 2 shows data on several materials, specifically on temperature-dependent electrical conductivity of oxides and some other materials [29]. Abrupt changes appear at well-defined temperatures and originate from structural transformations. Vanadium dioxide (VO_2) is of special interest since $\tau_c \approx 68$ °C, i.e., it is not vastly different from ordinary room temperature, as was discovered almost 60 years ago [47]. This material hence is the most

promising alternative for developing TC glazings and, in fact, most research efforts for this application make use of VO_2, at least as a point of departure. The switching at τ_c takes place between two states: (i) a low-temperature semiconducting phase characterized by low infrared absorption—and therefore large infrared throughput as a thin film—and monoclinic crystal structure; and (ii) a high-temperature metal-like phase having large infrared reflectance and rutile-type crystal structure. The physical nature of the switching at τ_c has been debated for decades and continues to be the subject of scientific inquiry as apparent from an ongoing steady stream of publications [48–51].

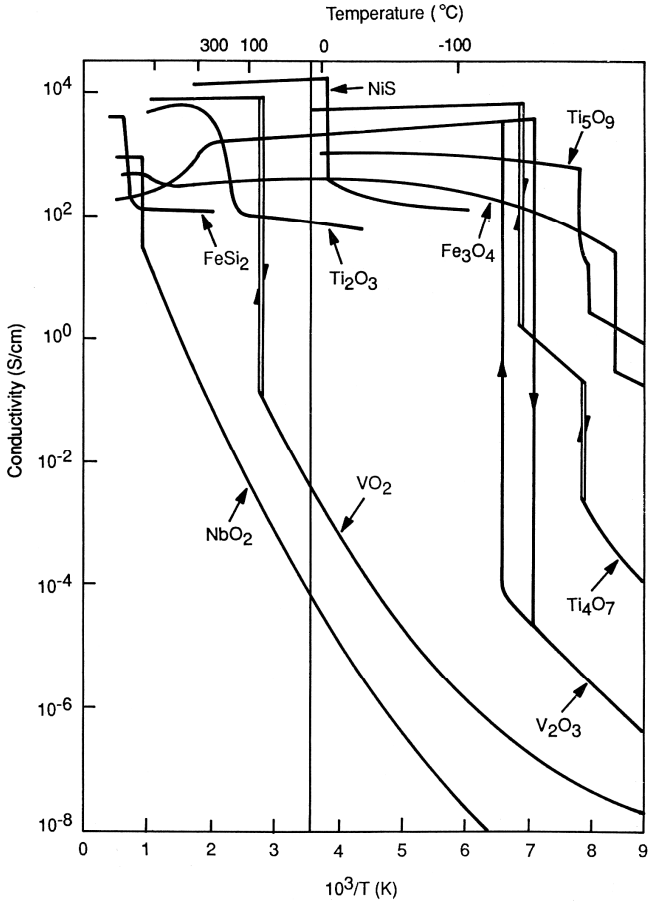

Figure 2. Electrical conductivity as a function of reciprocal temperature (lower horizontal axis) and temperature (upper horizontal axis) for the shown metal-based compounds. The vertical line denotes room temperature. Arrows on the vertical lines signify hysteretic transitions [29].

Figure 3 summarizes the most important optical properties of VO_2 thin films and nanoparticle composites. Figure 3a,c show spectral transmittance (a) and reflectance (c) for 50 nm-thick VO_2 films on glass for wavelengths pertinent to solar radiation. It is apparent that $T(\lambda,\tau)$ is much higher in the semiconducting state below τ_c than in the metallic state above τ_c as long as $\lambda > 1$ μm. The difference in the transmittance between low and high temperature is enhanced for increasing wavelength. This type of variation in $T(\lambda,\tau)$ clearly is the desired one, and a glazing with a VO_2-based TC thin film transmits more energy below τ_c than above τ_c. Similar properties have been recorded many times [31–40,52–54]. Figure 3 also demonstrates that corresponding data on $R(\lambda)$ increase monotonically towards long wavelengths for the metallic-like state above τ_c, which is the expected behavior. The reflectance seems to level off at ~40% for the 50 nm-thick film, and a higher reflectance would have been reached in a thicker film. Figure 3b,d apply to a dilute suspension of VO_2 nanospheres with a mass thickness of 50 nm. Comparing these data with those for the film and the solar spectrum in Figure 1 makes it

evident that $T_{lum}(\tau)$ and ΔT_{sol} are enlarged and that $R_{lum}(\tau)$ and $R_{sol}(\tau)$ are decreased and almost temperature-independent. These results will be discussed in more detail in Section 4 below.

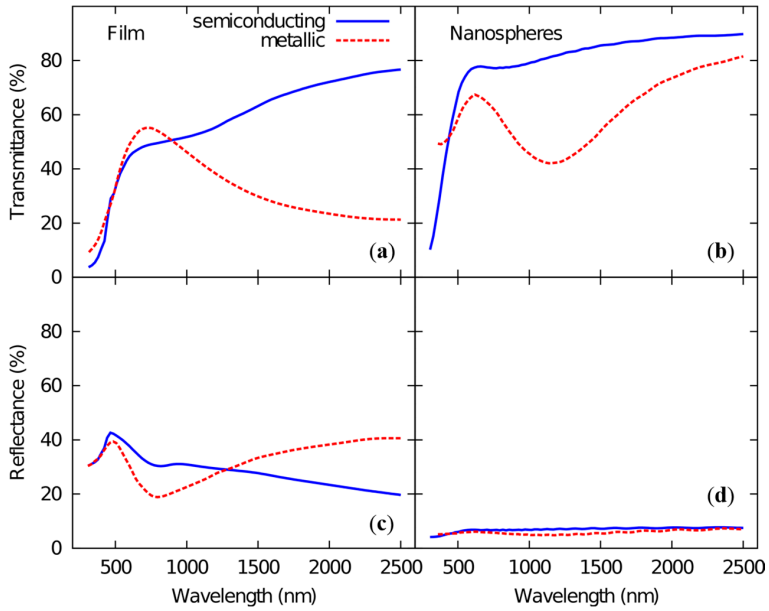

Figure 3. Spectral transmittance (**a**,**b**) and reflectance (**c**,**d**) for a 50 nm-thick thin film of VO_2 (**a**,**c**) and for a layer comprising a dilute dispersion of VO_2 nanospheres, with an equivalent VO_2 thickness of 50 nm, in a medium mimicking transparent glass or polymer (**b**,**d**).

3. On the Preparation of Vanadium Dioxide (VO_2) Thin Films and Nanoparticles

Techniques for making VO_2 thin films and nanoparticles are of much interest and are presently undergoing rapid development. Vanadium has high oxygen affinity and is able to form compounds with the metal in oxidation states being +5, +4, +3 and +2. Therefore, it is hardly surprising that the vanadium–oxygen phase diagram, shown in Figure 4, is complex and includes almost 20 different phases, frequently with only minor compositional differences [55–58]. The challenges for the synthesis of VO_2 are related to the co-existence of these various oxide forms and also with the existence of various polymorphs. Therefore, it is rarely straightforward to make phase-pure VO_2, which is produced in a very narrow interval of oxygen partial pressure.

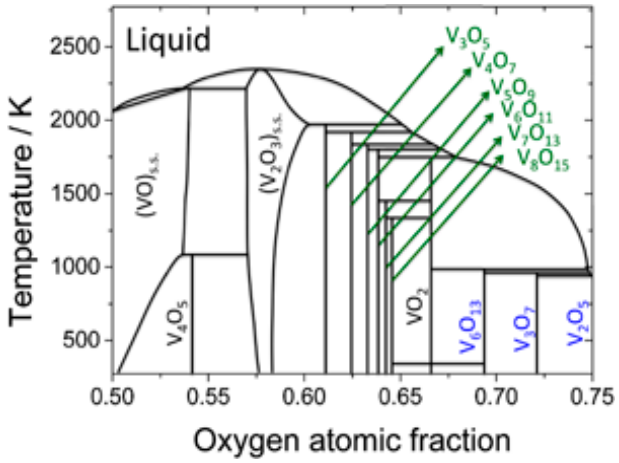

Figure 4. Phase diagram for the VO–$VO_{2.5}$ system [57].

Elemental solid (s) vanadium reacts with oxygen gas (g) in a simple and direct manner and yields VO_2 via the overall reaction

$$V(s) + O_2(g) \rightarrow VO_2(s). \quad (3)$$

This reaction constitutes the basis for various physical vapor deposition techniques—such as thermal evaporation [59], pulsed laser deposition [60] and sputtering [40,61,62]—which synthesize VO_2 thin films by deposition in an ambience with controlled oxygen partial pressure and at high temperature. The temperature is typically ~450 °C although lower temperatures can be used for special sputtering techniques employing pulsed plasma [63–67]. The required process control is difficult, and vanadium is rapidly oxidized at high temperature and transforms from tetragonal VO_2 to V_6O_{13} and V_3O_7, and it ultimately reaches thermodynamically stable orthorhombic V_2O_5 in agreement with the phase diagram in Figure 4 (we come back to this point in Section 4).

More facile thin-film preparation might be accomplished by use of a mild oxidation agent that could serve as an alternative to the oxygen in reaction (3). One possibility is to use SO_2, as discussed recently [40,62], in order to exploit the overall reaction

$$V(s) + SO_2(g) \rightarrow VO_2(s) + S(g), \quad (4)$$

presumably in conjunction with a catalyst for boosting the kinetics. If SO_2 is fully decomposed, the reaction products would be VO_2 and S; the sulfur can then be removed through vaporization at a high-enough temperature.

There are numerous other methods to manufacture VO_2-based thin films for glazings, such as chemical vapor deposition [68,69] and sol–gel technology [70]. Several of the deposition techniques were surveyed recently [54].

We now focus on VO_2-based nanoparticles, which can be prepared by a number of techniques, physical as well as chemical. This large body of work is cited, for example, in References [61,71]. Recent work has demonstrated that VO_2 nanoparticles can be prepared by direct and continuous synthesis via a two-step process incorporating hydrothermal flow synthesis followed by a short heat-treatment step [72]. Nanoparticles can be more or less well rounded and they can also be rod- and wire-like. Figure 5 shows scanning electron microscopy (SEM) images of nanorods prepared by sputter deposition onto glass heated to ~460 °C in an atmosphere of of oxygen and argon [61]. We focus on sputtering since this technique has excellent scalability and is commonly employed for glazing applictions.

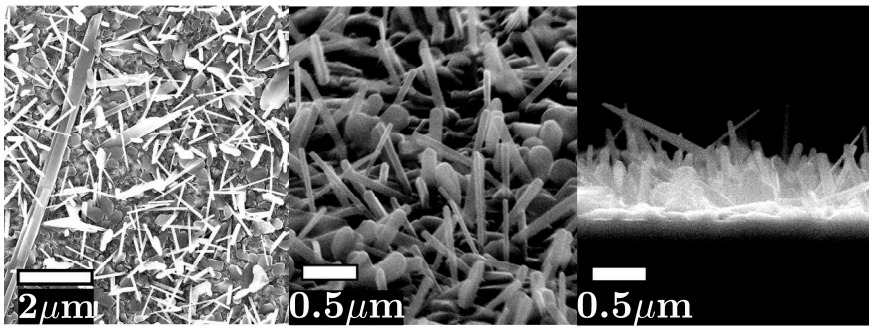

(**a**) (**b**) (**c**)

Figure 5. Scanning electron microscopy (SEM) images of a VO_2 layer deposited onto heated glass to an (equivalent) thickness of 102 nm. (**a**–**c**) images indicate a top-view, imaging with 70° between the electron beam and the sample's normal, and a cross-sectional picture, respectively. Note that the magnifications are different among the images [61].

The substrate material can have a significant influence on the growth of sputter-deposited particles [73], and glass precoated with electrically conducting In_2O_3:Sn (indium–tin oxide, ITO)

gave more well-defined particles than in the case of analogous deposition onto bare glass or glass precoated with non-conducting SnO_2. The reason for the influence of the substrate is not known in detail, but surface energy and the fact that an electrically conducting substrate avoids charge-induced repulsion between adjacent particles are expected to play a role. The sublayer of ITO on the glass substrate is of significance also because it broadens the process window for making VO_2 deposits with TC properties. Figure 6 shows images taken by SEM and atomic force microscopy (AFM) of a particulate VO_2 film on ITO-coated glass and demonstrates a layer of highly irregular nanoparticles with sizes of the order of 1 μm [74]; we come back to these films in Section 5 below.

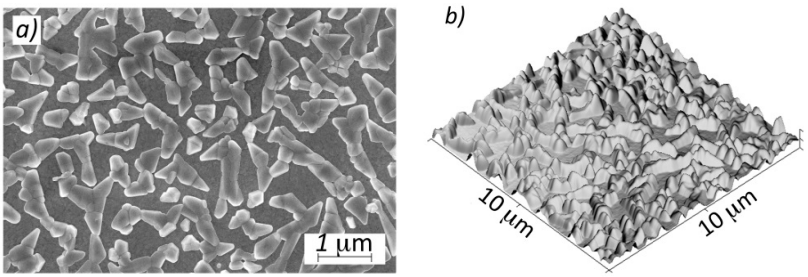

Figure 6. SEM top-view (**a**) and atomic force microscopy (AFM) image (**b**) of a particulate VO_2 layer on ITO-coated glass. The maximum peak height of the deposit was ~190 nm [74].

It is possible to embed the VO_2 nanoparticles in a host material, and Figure 7 shows preliminary results on a VO_2–SiO_2 composite prepared by reactive magnetron sputtering [75]. SEM micrographs displayed rounded nanoparticles with sizes of 100–300 nm, and energy-dispersive X-ray (EDX) studies indicated that these particles were vanadium-rich. In the case of an alternative deposition process, tiny VO_2-based crystallites were formed in an Al_2O_3 matrix by reactive co-sputtering onto a substrate kept at ~400 °C, as evidenced by the high-resolution transmission electron microscopy (HRTEM) image in Figure 8 [76].

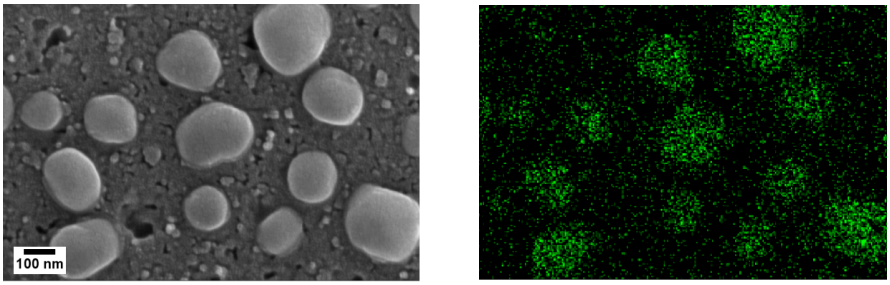

(**a**) (**b**)

Figure 7. SEM (**a**) and energy-dispersive X-ray (EDX) (**b**) data for a 220 nm-thick VO_2–SiO_2 film prepared by sputter deposition; green dots signify vanadium [75].

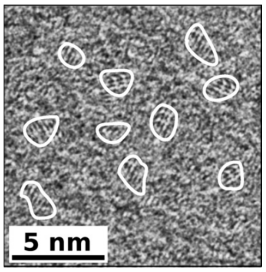

Figure 8. High-resolution transmission electron microscopy (HRTEM) image of a nanocrystalline VO_2–Al_2O_3 composite film with encircled areas indicating VO_2 [76].

Vanadium-dioxide-based thin films and nanoparticle composites for buildings integration are normally backed by rigid glass plates or panes. However, thin films can be prepared also on ultrathin flexible glass and on temperature-resistent polymer foil [65].

4. Towards VO_2-Based Thin Films for Glazings

The data for $T(\lambda,\tau)$ in the left-hand images of Figure 3 are interesting with regard to glazings, but the performance is hardly sufficient for practical implementation in buildings. Nevertheless, the properties of VO_2 are sufficiently near to the wanted ones that it makes good sense to make a concerted attempt to modify this material [32]. In particular, the following items demand careful consideration for VO_2-based coatings and are discussed in the remainder of the present section: (i) τ_c takes place at ~68 °C which clearly is too high for buildings; (ii) T_{lum} is only ~40% and too low for most glazings (T_{lum} would be higher for a thinner film but the consequence is then that ΔT_{sol} becomes minuscule); (iii) temperature-dependent transmittance modulation is large mainly for wavelengths where the solar irradiation is weak and this limits ΔT_{sol} to no more than ~10%; and (iv) VO_2 is not thermodynamically stable but further oxidation leads to non-TC V_2O_5.

We first consider whether τ_c can occur around room temperature. In fact, it was well known already in the early 1970s that an addition of tungsten and a number of other elements to bulk VO_2 can give a depression of τ_c [77–79], and the same effect can be found in thin films [80]. Other additions can enhance τ_c to some extent [77]. Figure 9 reports that ~2% of W displaces τ_c to approximately room temperature [81], and numerous other datasets give analogous results provided that the oxide film is well crystallized and homogeneous [32].

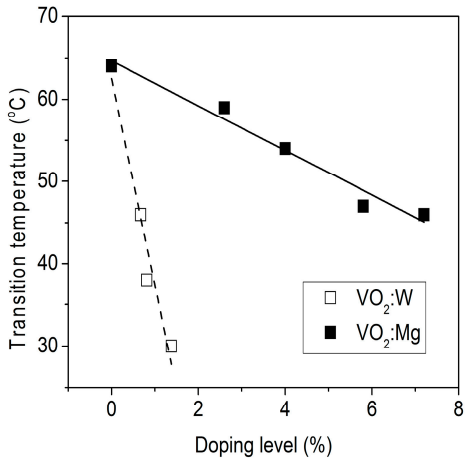

Figure 9. Transition termperature τ_c between semiconducting and metallic-like states in VO_2 films containing W or Mg [81]. The data are based on electrical measurements.

Next we look at ways to increase T_{lum}, or rather to lower the absorptance of visible light. Figure 3 demonstrates that strong optical absorption occurs at wavelengths below 0.5–0.6 μm, which is related to the fact that the optical band gap in VO_2 is smaller than desired. A partial solution to this problem can be reached by replacing some of the vanadium by magnesium [81–85] in order to widen the optical band gap, and this effect can be reconciled with computational results [86,87]. Figure 10 illustrates the effect of Mg doping by showing the spectral transmittance for 50 nm-thick films of doped and pure VO_2 at $\tau < \tau_c$ and $\tau > \tau_c$. It is evident that the dopant displaces the high-transmittance region towards shorter wavelengths, but it also has the unwanted effect of diminishing ΔT_{sol}. It is apparent from Figure 10 that τ_c drops as the Mg content is enhanced albeit not as rapidly as for W doping. Figure 11 indicates that T_{lum} is increased from 39% to 51% as the amount of Mg goes from zero to 7.2%. Band-gap widening can be accomplished also by adding other alkaline earth metals [83], zinc [88] or terbium [89], or by replacing some of the oxygen with fluorine [90–92].

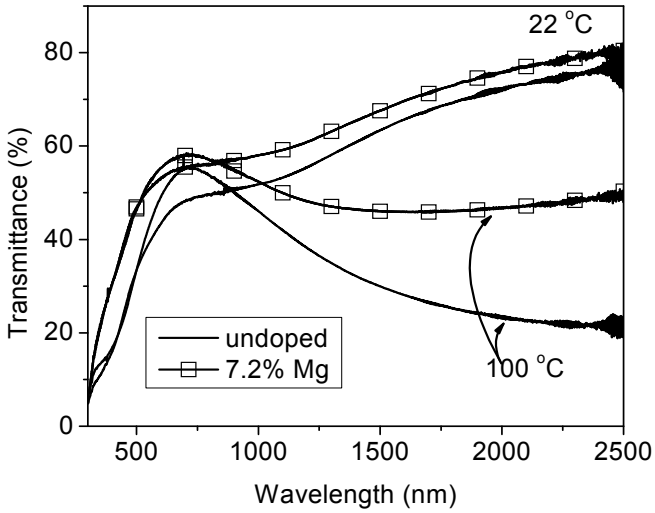

Figure 10. Spectral transmittance for 50 nm-thick Mg-doped and undoped VO_2 films in semiconducting (τ = 22 °C) and metallic (τ = 100 °C) states [81].

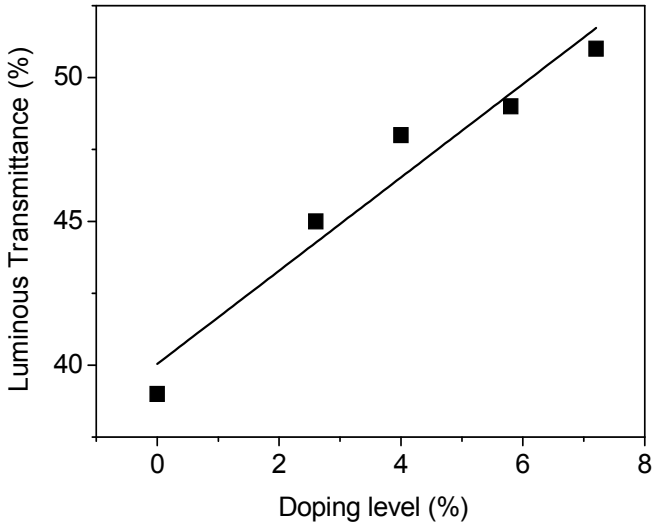

Figure 11. Luminous transmittance as a function of Mg doping in 50 nm-thick VO_2-based films as measured at τ = 22 °C. Line was drawn to guide the eye [81].

The third item under scrutiny is how to enhance ΔT_{sol}. An important step towards this goal was taken when it was discovered through computing that a layer of VO_2 nanoparticles—rather than a corresponding continuous thin film of this material—could yield the wanted properties [71,93]. Additional calculations showed that the particle size should not be larger than ~20 nm in order to prevent optical scattering ("haze") [94]. However, refractive-index-matching between VO_2 nanoparticles and an embedding material—as seen in Figure 7—can suppress scattering efficiently. "Nanothermochromism" [71] is in fact demonstrated in Figure 3b,d, which illustrate $T(\lambda)$ and $R(\lambda)$ for a 5 μm-thick layer of a transparent medium, whose refractive index is characteristic of glass and polymers, including 1 vol.% of well-dispersed and non-scattering nanospheres of VO_2. This choice of parameters produces an equivalent VO_2 thickness of 50 nm so that that the data for the nanospheres and for the continuous thin film can be readily compared.

Judging from Figure 3, it is clear that there are important qualitative differences between optical data for the nanoparticle composites and the corresponding thin films. Thus (i) the nanosphere-containing material is considerably more transparent than the corresponding thin film;

(ii) metallic-like nanoparticles display a clear-cut minimum in the transmittance for the $0.7 < \lambda < 1.5$ μm wavelength interval which strongly limits T_{sol} since the solar irradiance is intense for these wavelengths, whereas the visible optical performance is barely affected at all; and (iii) the nanospheres absorb rather than reflect. The striking transmittance minimum—which corresponds to an absorption maximum—in the infrared is due to localized plasmon resonance of free electrons in VO_2 nanoparticles and takes place around $\lambda \approx 1.2$ μm. Clearly, this feature has an almost ideal position for absorbing infrared solar radiation without influencing the visible performance (cf. Figure 1). A plasmonic character of the near-infrared absorption has been observed and discussed several times in prior work [95–98].

Figure 12 gives clear evidence for nanothermochromism in a film comprised of VO_2–SiO_2 and was recorded on the sample illustrated in Figure 7. The spectral absorptance $A(\lambda)$, derived according to

$$A(\lambda) = 1 - T(\lambda) - R(\lambda), \quad (5)$$

displays a conspicuous maximum for near-infrared solar radiation when the VO_2 nanoparticles are in their metallic-like state at $\tau > \tau_c$, whereas no feature of this kind can be discerned for the semiconductor state at $\tau < \tau_c$ [75].

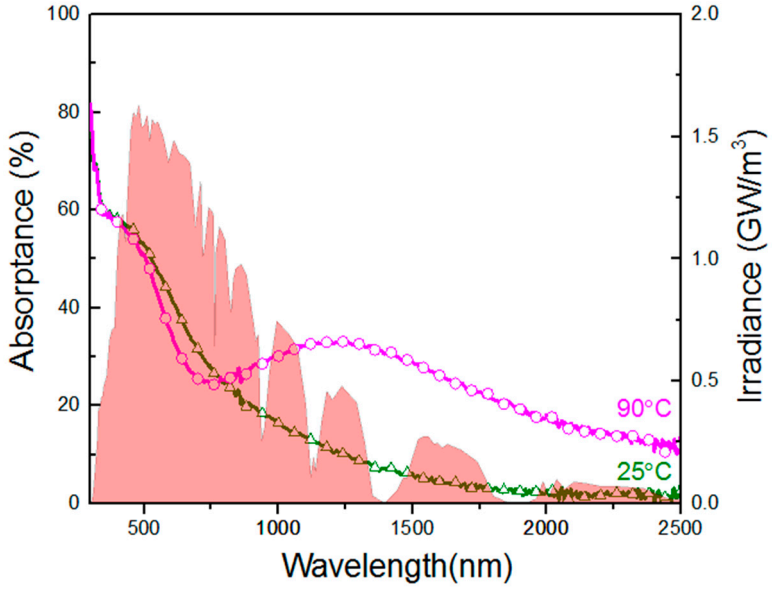

Figure 12. Spectral absorptance for the VO_2–SiO_2 deposit shown in Figure 7 as recorded at the stated temperatures. Also shown is a solar spectrum analogous to that in Figure 1b [75].

It is evident that various combinations of T_{lum} and ΔT_{sol} can be obtained in VO_2-based materials, and Figure 13 illustrates the current state of the art for $T_{lum}(\tau < \tau_c)$ and ΔT_{sol} [34]. It should be pointed out that T_{lum} is approximately the same at $\tau < \tau_c$ and $\tau > \tau_c$. Thin films of pure VO_2 give the lowest magnitudes of $T_{lum}(\tau < \tau_c)$ and ΔT_{sol}, but the optical performance can be boosted by antireflection (AR) layers. Particularly good properties were obtained with multilayers of TiO_2 and VO_2 [99–101]. "Bio-inspired" cone-shaped surfaces represent another possibility to increase T_{lum} [102]. Mg-containing VO_2 films have improved properties, which can be further enhanced by AR layers. However, optimum performance can be reached with VO_2 nanoparticles which, for example, can yield $T_{lum}(\tau < \tau_c) \approx 60\%$ and $\Delta T_{sol} > 20\%$. It is also seen that Mg-doped nanoparticles are not superior to nanoparticles of pure VO_2; the reason for this behavior is that the doping lowers the solar modulation, as seen in Figure 10, to a degree that is not balanced by the higher short-wavelength transmittance. Nanothermochromism is in a state of rapid development and, for example, recent work has demonstrated excellent TC properties in composite films comprised of VO_2 nanoparticles and ionic-liquid–nickel–chlorine complexes [103].

VO_2-based core–shell particles arranged so as to make two-dimensional photonic crystals can achieve static tunability of T_{lum} while thermochromism is exhibited with regard to T_{sol} [104].

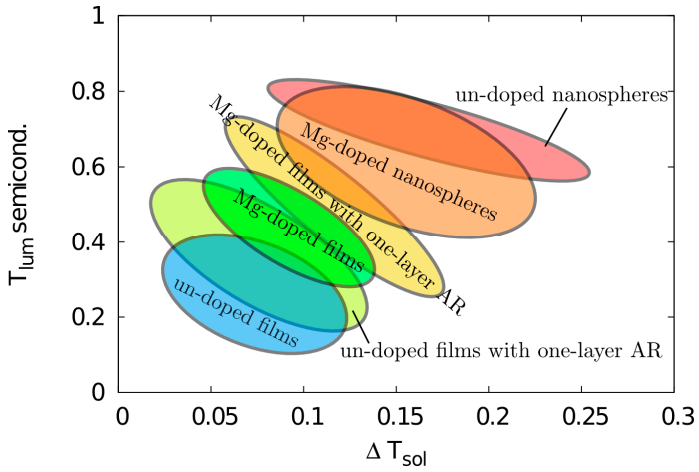

Figure 13. Schematic performance limits for VO_2-based thin films and nanoparticle composites with regard to TC glazings [34].

Finally, we look at the durability of VO_2-based thin films and nanoparticles, which is an issue of great practical interest since glazings must last for many years without essential performance losses. It must be remembered that V_2O_5 is thermodynamically stable, as is apparent from the phase diagram in Figure 4. Figure 14 reports data on 80 nm-thick sputter-deposited VO_2 thin films kept in dry air at 300 °C for one hour [105]. The as-deposited film demonstrates the expected TC properties (cf. Figures 3 and 10), whereas the heat-treated film displays a very different spectral transmittance which is indicative of non-TC V_2O_5 [106,107]. This transition is expected to be much slower at room temperature, but the data in Figure 14 nevertheless show that VO_2-based materials must be shielded against further oxidation. The durability of VO_2 is also dependent on the deposition technique and is improved for films with high density and large grain size [66,108].

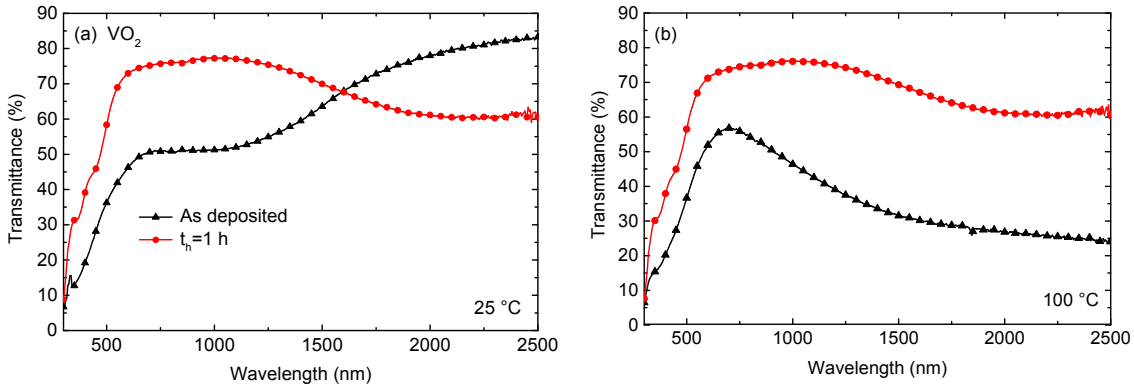

Figure 14. Spectral transmittance for an 80 nm-thick VO_2 film in as-deposited state and after subsequent heating at 300 °C for one hour. Data pertain to films in (**a**) semiconducting (τ = 25 °C) and (**b**) metallic-like (τ = 100 °C) states [105].

Figure 15 depicts $T(\lambda)$ for similar VO_2 films over-coated with 10 nm and 30 nm of sputter deposited alumina and heat treated at 300 °C for periods in the range $1 < t_h < 30$ h [105]. Clearly the top layer provides good protection, and only the thinnest Al_2O_3 layer and the longest heat-treatment period yielded some minor decline of the thermochromism. Al-nitride top layers were able to provide a similar

protection for VO_2 films [109]. The data in Figure 15 strongly indicate that VO_2-based materials can be used for long times in, for example, energy-efficient glazings. Over-coatings similar to the ones above gave efficient protection also under conditions of high humidity [105]. Recent work has demonstrated results that are similar to those above for the case of VO_2-based core–shell nanoparticles [110].

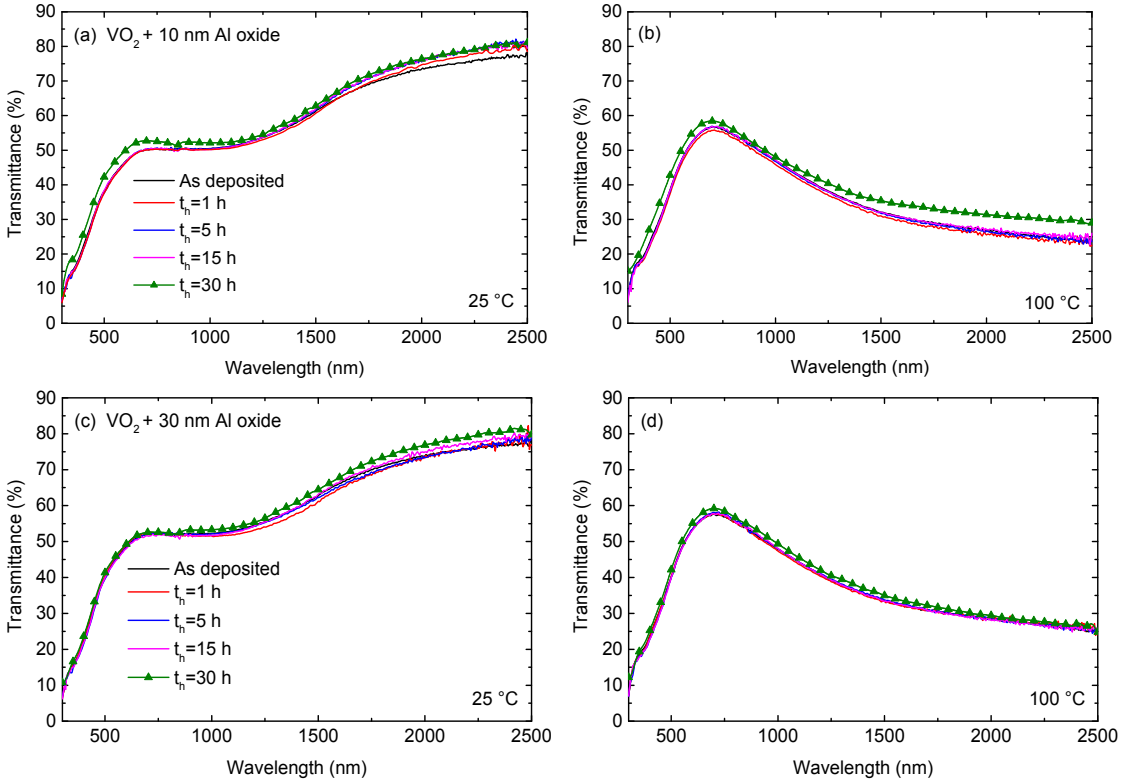

Figure 15. Spectral transmittance for 80 nm-thick VO_2 films, over-coated with 10 nm (**a**,**b**) and 30 nm (**c**,**d**) of Al_2O_3, in as-deposited state and after heating at 300 °C for the shown time periods t_h. Data were recorded for films in semiconducting (τ = 25 °C) and metallic-like (τ = 100 °C) states [105].

5. Recent Development: Thermochromic Light Scattering

Light scattering from VO_2 particles was investigated for samples with particle sizes of the order of 1 μm, which is comparable with the wavelengths for visible light and solar radiation. Specifically, the study employed the particulate layer depicted in Figure 6 [74], and the shown AFM image was quantified with regard to individual particle volumes V_p and surface areas S_p by use of available computer code [111]. In order to formulate a theoretical model of light-scattering data, the individual particles were modelled by use of two different sets of equivalent sphere radii: either equal-volume spheres represented by $r_{eq} = (3V_p/4\pi)^{1/3}$ or equal-volume-to-area spheres represented by $r'_{eq} = 3V_p/S_p$. Earlier work, rooted in atmospheric science, has demonstrated that the latter representation can work well for light scattering from highly irregular objects [112]. The particle number is not conserved in the latter case, and the number of equivalent spheres is larger than the number of real particles. Figure 16 presents actual data on the radial distributions for r_{eq} and r'_{eq}.

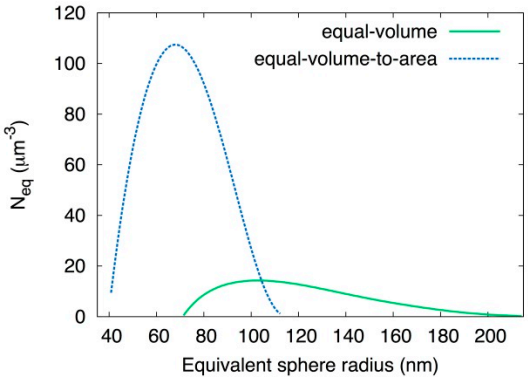

Figure 16. Distributions of the number N_{eq} of equivalent sphere radii for the data shown in Figure 6b [74].

Specular and diffuse reflectance as well as direct and diffuse transmittance were recorded at $\tau < \tau_c$ and $\tau > \tau_c$ for the particulate sample, and these results were used to derive approximate absorption and scattering coefficients—denoted α_{abs} and α_{sca}, respectively—as shown in Figure 17. Corresponding computed quantities—denoted K^*_{abs} and K^*_{sca}, respectively—were then obtained from Lorenz–Mie theory [113] applied to the particle radii distributions in Figure 16. It is evident from Figure 17 that the calculations based on the equal-volume-to-area model can be reconciled with experimental data at $\lambda < 0.7$ μm for absorption as well as scattering and at both low and high temperature. The equal-volume approximation worked less well. The conclusion is that a semi-quantitative description of TC light scattering appears possible even from highly irregular particles, but more work is needed to fully vindicate this result.

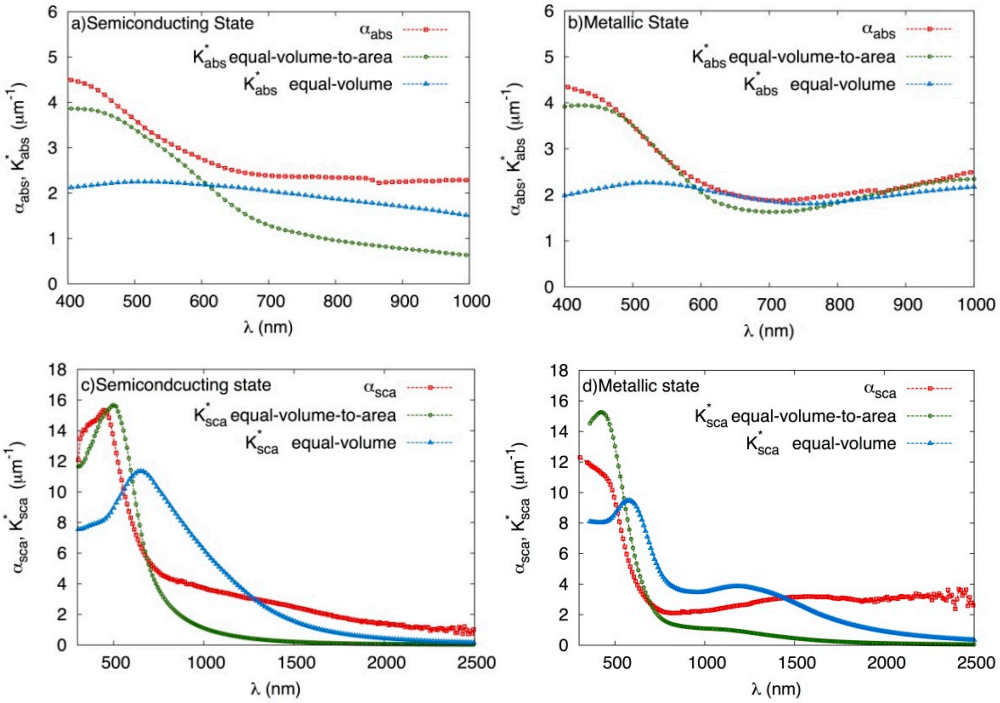

Figure 17. Experimental (α_{abs}) and theoretical (K^*_{abs}) spectral absorption data, and corresponding results for experimental (α_{sca}) and theoretical (K^*_{sca}) spectral scattering data, for the particulate VO_2 sample shown in Figure 6. The calculations used the equal-volume and equal-volume-to-area approximations in Figure 16. Data are given for the semiconducting state at $\tau < \tau_c$ (**a**,**c**) and the metallic state at $\tau > \tau_c$ (**b**,**d**) [74].

Glazing-related applications of TC light scattering can be envisaged, and other uses may include functional fibre mats [114,115] and elastomeric composites [116].

6. Conclusions

We have given an overview of recent progress on materials for thermochromic glazings for applications in energy-efficient buildings. The presentation was confined to VO_2-based thin coatings and nanoparticle composites, but it should be kept in mind that there are other thermochromic materials, especially among the organics [117,118]. In the case of vanadium dioxide (VO_2)-based thin films, switching occurs between states with low and high solar energy throughput at high and low temperature, respectively. The transition temperature can be brought close to room temperature by adding some tungsten atoms, and luminous transmittance can be enhanced by antireflection layers as well as by doping with magnesium. Nanoparticle composites with VO_2 dispersed in a transparent host are able to combine large luminous transmittance with a high modulation of solar energy transmittance. Durability under heating and at high humidity can be accomplished by use of protective over-coatings.

With regard to practical application in thermochromic glazings, VO_2-based thin films can be employed in insulated glass units in the same way as in current technology which normally uses metal-based or doped-semiconductor-based thin films with static optical properties [15,119]. The thin films must be produced by a method that allows large-scale high-throughput manufacturing, with reactive DC magnetron sputtering and chemical vapor deposition (spray pyrolysis) being established technologies. Thermochromic nanoparticles—probably with VO_2 cores surrounded by protective shells—can be dispersed in polymeric lamination materials. Another development may be to employ such thermochromic laminates as electrolytes in electrochromic devices capable of modulating the transmittance of visible light and solar energy when electrical charge is transported between thin films based on, for example, nickel oxide and tungsten oxide [120–122]. Furthermore, thermochromism can be combined with photocatalytic self-cleaning in multifunctional glazings [123].

We note, finally, that technologies such as those discussed in this article may lead to a radical change of the very concept of a building—it must no longer be static, and in need of vast quantities of energy to achieve an adequate indoor environment, but instead can be dynamic and able to adapt to varying ambience, thereby minimizing energy expenditure and enhancing indoor comfort.

Conflicts of Interest: The authors declare no conflict of interest.

References

1. U.S. Department of Commerce, National Oceanic and Atmospheric Administration, Earthscan System Research Laboratory, Global Monitoring Division. Available online: http://www.esrl.noaa.gov/gmd/ccgg/trends/index.html (accessed on 14 November 2016).
2. Stocker, T.F.; Qin, D.; Plattner, G.-K.; Tignor, M.M.B.; Allen, S.K.; Boschung, J.; Nauels, A.; Xia, Y.; Bex, V.; Midgley, P.M. (Eds.) *Climate Change 2013: The Physical Science Basis. Working Group I Contribution to the Fifth Assessment Report on the Intergovermental Panel on Climate Change*; Cambridge University Press: New York, NY, USA, 2013.
3. Burke, M.; Hsiang, S.M.; Miguel, E. Global non-linear effect of temperature on economic production. *Nature* **2015**, *527*, 235–239. [CrossRef] [PubMed]
4. Kelley, C.P.; Mohtadi, S.; Cane, M.A.; Seager, R.; Kushnir, Y. Climate change in the Fertile Crescent and implications of the recent Syrian drought. *Proc. Natl. Acad. Sci. USA* **2015**, *112*, 3241–3246. [CrossRef] [PubMed]
5. Carleton, T.A.; Hsiang, S.M. Social and economic impacts of climate. *Science* **2016**, *353*, aad9837/1–aad9837/15. [CrossRef] [PubMed]
6. United Nations, Department of Economic and Social Affairs. *World Population Prospects: The 2015 Revision*; United Nations: New York, NY, USA, 2015.
7. United Nations, Department of Economic and Social Affairs. *World Urbanization Prospects: The 2014 Revision*; United Nations: New York, NY, USA, 2014.

8. Akbari, H.; Cartalis, C.; Kolokotsa, D.; Muscio, A.; Pisello, A.L.; Rossi, F.; Santamouris, M.; Synnefa, A.; Wong, N.H.; Zinzi, M. Local climate change and urban heat island mitigation techniques: The state of the art. *J. Civil Eng. Manag.* **2016**, *22*, 1–16. [CrossRef]
9. Sachindra, D.A.; Ng, A.W.M.; Muthukumaran, S.; Perera, B.J.C. Impact of climate change on urban heat island effect and extreme temperatures: A case-study. *Quart. J. R. Meterorol. Soc.* **2016**, *142*, 172–186. [CrossRef]
10. Waters, C.N.; Zalasiewicz, J.; Summerhayes, C.; Barnosky, A.D.; Poirer, C.; Galuszka, A.; Cearreta, A.; Edgeworth, M.; Ellis, E.C.; Ellis, M.; et al. The Antropocene is functionally and stratigraphically distinct from the Holocene. *Science* **2016**, *351*, aad2622/1–aad2622/10. [CrossRef] [PubMed]
11. United Nations Environmental Programme. *Buildings and Climate Change: Summary for Decision-Makers*; UNDP Sustainable Buildings & Climate Initiative: Paris, France, 2009.
12. U.S. Department of Energy. *2011 Buildings Energy Data Book*; U.S. Department of Energy: Washington, DC, USA, 2012.
13. Leech, J.A.; Nelson, W.C.; Burnett, R.T.; Aaron, S.; Raizenne, M.E. It's about time: A comparison of Canadian and American time–activity patterns. *J. Exposure Anal. Environm. Epidemiol.* **2002**, *12*, 427–432. [CrossRef] [PubMed]
14. Richter, B.; Goldston, D.; Crabtree, G.; Glicksman, L.; Goldstein, D.; Greene, D.; Kammen, D.; Levine, M.; Lubell, M.; Savitz, M.; et al. How America can look within to achieve energy security and reduce global warming. *Rev. Mod. Phys.* **2008**, *80*, S1–S107. [CrossRef]
15. Smith, G.B.; Granqvist, C.G. *Green Nanotechnology: Solutions for Sustainability and Energy in the Built Environment*; CRC Press: Boca Raton, FL, USA, 2010.
16. Ginley, D.S.; Cahen, D. (Eds.) *Fundamentals of Materials for Energy and Environmental Sustainability*; Cambridge University Press: Cambridge, UK, 2012.
17. García-Martínez, J. (Ed.) *Nanotechnology for the Energy Challenge*; Wiley-VCH: Weinheim, Germany, 2013.
18. Pacheco-Torgal, F.; Diamanti, M.V.; Nazari, A.; Granqvist, C.G. (Eds.) *Nanotechnology in Eco-Efficient Construction*; Woodhead: Cambridge, UK, 2013.
19. Pacheco-Torgal, F.; Mistretta, M.; Kaklauskas, A.; Granqvist, C.G.; Cabeza, L.F. (Eds.) *Nearly Zero Energy Building Refurbishment*; Springer: London, UK, 2013.
20. Pacheco-Torgal, F.; Labrincha, J.A.; Cabeza, L.F.; Granqvist, C.G. (Eds.) *Eco-Efficient Materials for Mitigating Building Cooling Needs: Design, Properties and Applications*; Woodhead: Cambridge, UK, 2015.
21. Pacheco-Torgal, F.; Buratti, C.; Kalaiselvam, S.; Granqvist, C.G.; Ivanov, V. (Eds.) *Nano and Biotech Based Materials for Energy Building Efficiency*; Springer: Cham, Switzerland, 2016.
22. Pacheco-Torgal, F.; Rasmussen, E.; Granqvist, C.G.; Ivanov, V.; Kaklauskas, A.; Makonin, S. (Eds.) *Start-Up Creation: The Smart Eco-Efficient Built Environment*; Woodhead: Cambridge, UK, 2016.
23. Pacheco-Torgal, F.; Granqvist, C.G.; Jelle, B.P.; Vanoli, G.P.; Bianco, N.; Kurnitski, J. (Eds.) *Cost-Effective Energy Efficient Building Retrofitting: Materials, Technologies, Optimization and Case Studies*; Woodhead: Cambridge, UK, 2017.
24. Heschong, L.; Wright, R.L.; Okura, S. Daylighting impacts on retail sales performance. *J. Illum. Engr. Soc.* **2002**, *31*, 21–25. [CrossRef]
25. Heschong, L.; Wright, R.L.; Okura, S. Daylighting impacts on human performance in school. *J. Illum. Engr. Soc.* **2002**, *31*, 101–114. [CrossRef]
26. Altomonte, S. Daylight for energy savings and psycho-physiological well-being in sustainable built environments. *J. Sustain. Dev.* **2008**, *1*, 3–16. [CrossRef]
27. Granqvist, C.G. Chromogenic materials for transmittance control of large-area windows. *Crit. Rev. Solid State Phys. Mater. Sci.* **1990**, *16*, 291–308. [CrossRef]
28. Lampert, C.M.; Granqvist, C.G. (Eds.) *Large-Area Chromogenics: Materials and Devices for Transmittance Control*; SPIE Institutes for Advanced Optical Technologies; SPIE Optical Engineering Press: Bellingham, WA, USA, 1990; Volume IS4.
29. Jorgenson, G.V.; Lee, J.C. Doped vanadium oxide for optical switching films. *Sol. Energy Mater.* **1986**, *14*, 205–214. [CrossRef]
30. Babulanam, S.M.; Eriksson, T.S.; Niklasson, G.A.; Granqvist, C.G. Thermochromic VO_2 films for energy-efficient windows. *Sol. Energy Mater.* **1987**, *16*, 347–363. [CrossRef]

31. Gao, Y.; Luo, H.; Zhang, Z.; Kang, L.; Chen, Z.; Du, J.; Kanehira, M.; Cao, C. Nanoceramic VO_2 thermochromic smart glass: A review on progress in solution processing. *Nano Energy* **2012**, *1*, 221–246. [CrossRef]
32. Li, S.-Y.; Niklasson, G.A.; Granqvist, C.G. Thermochromic fenestration with VO_2-based materials: Three challenges and how they can be met. *Thin Solid Films* **2012**, *520*, 3823–3828. [CrossRef]
33. Li, S.-Y. *VO_2-Based Thermochromic and Nanothermochromic Materials for Energy-Efficient Windows: Computational and Experimental Studies*; Digital Comprehensive Summaries of Uppsala Dissertations from the Faculty of Science and Technology 1095; Acta Universitatis Upsaliensis: Uppsala, Sweden, 2013.
34. Li, S.-Y.; Niklasson, G.A.; Granqvist, C.G. Thermochromic undoped and Mg-doped VO_2 thin films and nanoparticles: Optical properties and performance limits for energy efficient windows. *J. Appl. Phys.* **2014**, *115*, 053513/1–053513/10. [CrossRef]
35. Hoffmann, S.; Lee, E.S.; Clavero, C. Examination of the technical potential of near-infrared switching thermochromic windows for commercial building applications. *Sol. Energy Mater. Sol. Cells* **2014**, *123*, 65–80. [CrossRef]
36. Warwick, M.E.A.; Binions, R. Advances in thermochromic vanadium dioxide films. *J. Mater. Chem. A* **2014**, *2*, 3275–3292. [CrossRef]
37. Anderson, A.-L.; Chen, S.; Romero, L.; Binions, R. Thin films for advanced glazing applications. *Buildings* **2016**, *6*, 37. [CrossRef]
38. Warwick, M.E.A.; Ridley, I.; Binions, R. Variation of thermochromic glazing systems transition temperature, hysteresis gradient and width on energy efficiency. *Buildings* **2016**, *6*, 22. [CrossRef]
39. Warwick, M.E.A.; Ridley, I.; Binions, R. Thermochromic vanadium dioxide thin films prepared by electric field assisted atmospheric pressure chemical vapour deposition for intelligent glazing application and their energy demand reduction properties. *Sol. Energy Mater. Sol. Cells* **2016**, *157*, 686–694. [CrossRef]
40. Ji, Y.-X.; Boman, M.; Niklasson, G.A.; Granqvist, C.G. Thermochromics for energy-efficient buildings: Thin surface coatings and nanoparticle composites. In *Nano and Biotech Based Materials for Energy Building Efficiency*; Pacheco-Torgal, F., Buratti, C., Kalaiselvam, S., Granqvist, C.G., Ivanov, V., Eds.; Springer: Cham, Switzerland, 2016; pp. 71–96.
41. The Freedonia Group. *World Flat Glass to 2016: Industry Market Research, Market Share, Market Size, Sales, Demand Forecast, Market Leaders, Company Profiles, Industry Trends*; The Freedonia Group: Cleveland, OH, USA, 2013.
42. Wyszecki, J.; Stiles, W.S. *Color Science: Concepts and Methods, Quantitative Data and Formulae*, 2nd ed.; Wiley: New York, NY, USA, 2000.
43. American Society for Testing and Materials (ASTM). American Society for Testing and Materials (ASTM). G173-03 Standard tables of reference solar spectral irradiances: Direct normal and hemispherical on a 37° tilted surface. In *Annual Book of ASTM Standards*; American Society for Testing and Materials: Philadelphia, PA, USA, 2012.
44. Granqvist, C.G. Oxide-based chromogenic coatings and devices for energy efficient fenestration: Brief survey and update on thermochromics and electrochromics. *J. Vac. Sci. Technol. B* **2014**, *32*, 060801/1–060801/13. [CrossRef]
45. Granqvist, C.G. Recent progress in thermochromics and electrochromics: A brief survey. *Thin Solid Films* **2016**, *614*, 90–96. [CrossRef]
46. Granqvist, C.G.; Ji, Y.-X.; Montero, J.; Niklasson, G.A. Thermochromic vanadium-dioxide-based thin films and nanoparticles: Survey of some buildings-related advances. *J. Phys. Conf. Ser.* **2016**, *764*, 012002/1–012002/11. [CrossRef]
47. Morin, F.J. Oxides which show a metal-to-insulator transition at the Neel temperature. *Phys. Rev. Lett.* **1959**, *3*, 34–36. [CrossRef]
48. Chen, S.; Liu, J.; Luo, H.; Gao, Y. Calculation evidence of staged Mott and Peierls transitions in VO_2 revealed by mapping reduced-dimension potential energy surface. *Phys. Chem. Lett.* **2015**, *6*, 3650–3656. [CrossRef] [PubMed]
49. Zheng, H.; Wagner, L.K. Computation of the correlated metal–insulator transition in vanadium dioxide from first principles. *Phys. Rev. Lett.* **2015**, *114*, 176401/1–176401/4. [CrossRef] [PubMed]
50. Kumar, S.; Strachan, J.P.; Kilcoyne, A.L.D.; Tyliszczak, T.; Pickett, M.D.; Santori, C.; Gibson, G.; Williams, R.S. The phase transition in VO_2 probed using X-rays, visible and infrared radiations. *Appl. Phys. Lett.* **2016**, *108*, 073102/1–073102/4. [CrossRef]

51. Liu, S.; Phillabaum, B.; Carlson, E.W.; Dahmen, K.A.; Vidhyadhiraja, N.S.; Qazilbash, M.M.; Basov, D.N. Random field driven spatial complexity at the Mott transition in VO_2. *Phys. Rev. Lett.* **2016**, *116*, 036401/1–036401/5. [CrossRef] [PubMed]
52. Saeli, M.; Piccirillo, C.; Parkin, I.P.; Binions, R.; Ridley, I. Energy modelling studies of thermochromic glazing. *Energy Build.* **2010**, *42*, 1666–1673. [CrossRef]
53. Saeli, M.; Piccirillo, C.; Parkin, I.P.; Ridley, I.; Binions, R. Nano-composite thermochromic thin films and their application in energy-efficient glazing. *Sol. Energy Mater. Sol. Cells* **2010**, *94*, 141–151. [CrossRef]
54. Wang, S.; Liu, M.; Kong, L.; Long, Y.; Jiang, X.; Yu, A. Recent progress in VO_2 smart coatings: Strategies to improve the thermochromic properties. *Progr. Mater. Sci.* **2016**, *81*, 1–54. [CrossRef]
55. Smith, J.F. (Ed.) Phase diagrams of binary vanadium alloys. In *Monograph Series on Alloy Phase Diagrams*; ASM International: Metals Park, OH, USA, 1989.
56. Wriedt, H.A. The O–V (oxygen–vanadium) system. *Bull. Alloy Phase Diagr.* **1989**, *10*, 271–277. [CrossRef]
57. Kang, Y.-B. Critical evaluation and thermodynamic optimization of the VO–$VO_{2.5}$ system. *J. Eur. Ceram. Soc.* **2012**, *32*, 3187–3198. [CrossRef]
58. Bahlawane, N.; Lenoble, D. Vanadium oxide compounds: Structure, properties, and growth from the gas phase. *Chem. Vapor Depos.* **2014**, *20*, 299–311. [CrossRef]
59. Marvel, R.E.; Appavoo, K.; Choi, B.K.; Nag, J.; Haglund, R.F., Jr. Electron-beam deposition of vanadium dioxide thin films. *Appl. Phys. A* **2013**, *111*, 975–981. [CrossRef]
60. Jian, J.; Chen, A.; Zhang, W.; Wang, H. Sharp metal-to-insulator transition of VO_2 thin films on glass substrates. *J. Appl. Phys.* **2013**, *114*, 244301/1–244301/6. [CrossRef]
61. Li, S.-Y.; Namura, K.; Suzuki, M.; Niklasson, G.A.; Granqvist, C.G. Thermochromic VO_2 nanorods made by sputter deposition: Growth conditions and optical modeling. *J. Appl. Phys.* **2013**, *114*, 033516/1–033516/11. [CrossRef]
62. Ji, Y.-X.; Niklasson, G.A.; Granqvist, C.G.; Boman, M. Thermochromic VO_2 films by thermal oxidation of vanadium in SO_2. *Sol. Energy Mater. Sol. Cells* **2016**, *144*, 713–716. [CrossRef]
63. Fortier, J.-P.; Baloukas, B.; Zabeida, O.; Klemberg-Sapieha, J.E.; Martinu, L. Thermochromic VO_2 thin films deposited by HiPIMS. *Sol. Energy Mater. Sol. Cells* **2014**, *125*, 291–296. [CrossRef]
64. Aijaz, A.; Ji, Y.-X.; Montero, J.; Niklasson, G.A.; Granqvist, C.G.; Kubart, T. Low-temperature synthesis of thermochromic vanadium dioxide thin films by reactive high power impulse magnetron sputtering. *Sol. Energy Mater. Sol. Cells* **2016**, *149*, 137–144. [CrossRef]
65. Loquai, S.; Baloukas, B.; Zabeida, O.; Klemberg-Sapieha, J.E.; Martinu, L. HiPIMS-deposited thermochromic VO_2 films on polymeric substrates. *Sol. Energy Mater. Sol. Cells* **2016**, *155*, 60–69. [CrossRef]
66. Loquai, S.; Baloukas, B.; Klemberg-Sapieha, J.E.; Martinu, L. HiPIMS-deposited thermochromic VO_2 films with high environmental stability. *Sol. Energy Mater. Sol. Cells* **2017**, *160*, 217–224. [CrossRef]
67. Houska, J.; Kolenaty, D.; Rezek, J.; Vlcek, J. Characterization of thermochromic VO_2 (prepared at 250 °C) in a wide temperature range by spectroscopic ellipsometry. *Appl. Surf. Sci.* **2017**, in press. [CrossRef]
68. Drosos, C.; Vernardou, D. Perspectives of energy materials grown by APCVD. *Sol. Energy Mater. Sol. Cells* **2015**, *140*, 1–8. [CrossRef]
69. Louloudakis, D.; Vernardou, D.; Spanakis, E.; Suchea, M.; Kenanakis, G.; Pemble, M.; Savvakis, C.; Katsarakis, N.; Koudoumas, E.; Kiriakidis, G. Atmospheric pressure chemical vapor deposition of amorphous tungsten doped vanadium dioxide for smart window applications. *Adv. Mater. Lett.* **2016**, *7*, 10–15. [CrossRef]
70. Seyfouri, M.M.; Binions, R. Sol–gel approaches to thermochromic vanadium dioxide coating for smart glazing application. *Sol. Energy Mater. Sol. Cells* **2017**, *159*, 52–65. [CrossRef]
71. Li, S.-Y.; Niklasson, G.A.; Granqvist, C.G. Nanothermochromics: Calculations for VO_2 nanoparticles in dielectric hosts show much improved luminous transmittance and solar energy transmittance modulation. *J. Appl. Phys.* **2010**, *108*, 063525/1–063525/5. [CrossRef]
72. Powell, M.J.; Marchand, P.; Denis, C.J.; Bear, J.C.; Darr, J.A.; Parkin, I.P. Direct and continuous synthesis of VO_2 nanoparticles. *Nanoscale* **2015**, *7*, 18686–18693. [CrossRef] [PubMed]
73. Montero, J.; Ji, Y.-X.; Li, S.-Y.; Niklasson, G.A.; Granqvist, C.G. Sputter deposition of thermochromic VO_2 films on In_2O_3:Sn, SnO_2 and glass: Structure and composition versus oxygen partial pressure. *J. Vac. Sci. Technol. B* **2015**, *33*, 031805/1–031804/7. [CrossRef]
74. Montero, J.; Ji, Y.-X.; Granqvist, C.G.; Niklasson, G.A. Thermochromic light scattering from particulate VO_2 layers. *J. Appl. Phys.* **2016**, *119*, 085302/1–085302/6. [CrossRef]

75. Ji, Y.-X.; Niklasson, G.A.; Granqvist, C.G. Direct formation of thermochromic composite films of VO_2 nanoparticles in SiO_2 hosts. In Proceedings of the IEEE Nano 2016: 16th International Conference on Nanotechnology, Sendai, Japan, 22–26 August 2016; pp. 823–825.
76. Romanyuk, A.; Steiner, R.; Marot, L.; Spassov, V.; Oelhafen, P. nc-VO_2/Al_2O_3 nanocomposite films prepared by dual target magnetron sputtering. *Thin Solid Films* **2008**, *516*, 8513–8516. [CrossRef]
77. Goodenough, J.B. The two components of the crystallographic transition in VO_2. *J. Solid State Chem.* **1971**, *3*, 490–500. [CrossRef]
78. Hörlin, T.; Niklewski, T.; Nygren, M. Electrical and magnetic properties of $V_{1-x}W_xO_2$, $0 \leq x \leq 0.060$. *Mater. Res. Bull.* **1972**, *7*, 1515–1524. [CrossRef]
79. Reyes, J.M.; Lynch, G.F.; Sayer, M.; McBride, S.L.; Hutchison, T.S. Electrical, optical, magnetic resonance and microhardness properties of tungsten-doped VO_2. *J. Can. Ceram. Soc.* **1972**, *41*, 69–75.
80. Greenberg, C.B. Undoped and doped VO_2 films grown from $VO(OC_3H_7)_3$. *Thin Solid Films* **1983**, *110*, 7–82. [CrossRef]
81. Mlyuka, N.R.; Niklasson, G.A.; Granqvist, C.G. Mg doping of thermochromic VO_2 films enhances the optical transmittance and decreases the metal–insulator transition temperature. *Appl. Phys. Lett.* **2009**, *95*, 171909/1–171909/3. [CrossRef]
82. Li, S.-Y.; Mlyuka, N.R.; Primetzhofer, D.; Hallén, A.; Possnert, G.; Niklasson, G.A.; Granqvist, C.G. Bandgap widening in thermochromic Mg-doped VO_2 thin films: Quantitative data based on optical absorption. *Appl. Phys. Lett.* **2013**, *103*, 161907/1–161907/4. [CrossRef]
83. Dietrich, M.K.; Kramm, B.G.; Becker, M.; Meyer, B.K.; Polity, A.; Klar, P.J. Influence of doping with alkaline earth metals on the optical properties of thermochromic VO_2. *J. Appl. Phys.* **2015**, *117*, 185301/1–185301/8. [CrossRef]
84. Gagaoudakis, E.; Kortidis, I.; Michail, G.; Tsagaraki, K.; Binas, V.; Kiriakidis, G.; Aperathitis, E. Study of low temperature rf-sputtered Mg-doped vanadium dioxide thermochromic films deposited on low-emissivity substrates. *Thin Solid Films* **2016**, *601*, 99–105. [CrossRef]
85. Panagopoulou, M.; Gagaoudakis, E.; Boukos, N.; Aperathitis, E.; Kiriakidis, G.; Tsoukalas, D.; Raptis, Y.S. Thermochromic performance of Mg-doped VO_2 thin films on functional substrates for glazing applications. *Sol. Energy Mater. Sol. Cells* **2016**, *157*, 1004–1010. [CrossRef]
86. Hu, S.; Li, S.-Y.; Ahuja, R.; Granqvist, C.G.; Hermansson, K.; Niklasson, G.A.; Scheicher, R.H. Optical properties of Mg-doped VO_2: Absorption measurements and hybrid functional calculations. *Appl. Phys. Lett.* **2012**, *101*, 201902/1–201902/4.
87. Abdellaoui, I.; Merad, G.; Maaza, M.; Si Abdelkader, H. Electronic and optical properties of Mg-, F-doped and Mg/F-codoped M_1-VO_2 via hybrid density functional calculations. *J. Alloys Cpds.* **2016**, *658*, 569–575. [CrossRef]
88. Jiang, M.; Bao, S.; Cao, X.; Li, Y.; Li, S.; Zhou, H.; Luo, H.; Jin, P. Improved luminous transmittance and diminished yellow color in VO_2 energy efficient smart thin films by Zn doping. *Ceram. Int.* **2014**, *40*, 6331–6334. [CrossRef]
89. Wang, N.; Duchamp, M.; Dunin-Borokowski, R.E.; Liu, S.; Zeng, X.T.; Cao, X.; Long, Y. Terbium-doped VO_2 thin films: Reduced phase transition temperature and largely enhanced luminous transmittance. *Langmuir* **2016**, *32*, 759–764. [CrossRef] [PubMed]
90. Khan, K.A.; Granqvist, C.G. Thermochromic sputter-deposited vanadium oxyfluoride coatings with low luminous absorptance. *Appl. Phys. Lett.* **1989**, *55*, 4–6. [CrossRef]
91. Burkhardt, W.; Christmann, T.; Franke, S.; Kriegseis, W.; Meister, D.; Meyer, B.K.; Niessner, W.; Schalch, D.; Scharmann, A. Tungsten and fluorine co-doping of VO_2 films. *Thin Solid Films* **2002**, *402*, 226–231. [CrossRef]
92. Kiri, P.; Warwick, M.E.A.; Binions, B. Fluorine doped vanadium dioxide thin films for smart windows. *Thin Solid Films* **2011**, *520*, 1363–1366. [CrossRef]
93. Li, S.-Y.; Niklasson, G.A.; Granqvist, C.G. Nanothermochromics with VO_2-based core–shell structures: Calculated luminous and solar optical properties. *J. Appl. Phys.* **2011**, *109*, 113515/1–113515/8. [CrossRef]
94. Laaksonen, K.; Li, S.-Y.; Puisto, S.R.; Rostedt, N.K.J.; Ala-Nissila, T.; Granqvist, C.G.; Nieminen, R.M.; Niklasson, G.A. Nanoparticles of TiO_2 and VO_2 in dielectric media: Conditions for low optical scattering, and comparison between effective medium and four-flux theories. *Sol. Energy Mater. Sol. Cells* **2014**, *130*, 132–137. [CrossRef]

95. Lopez, R.; Boatner, L.A.; Haynes, T.E.; Feldman, L.C.; Haglund, R.F., Jr. Synthesis and characterization of size-controlled vanadium-dioxide nanocrystals in a fused silica matrix. *J. Appl. Phys.* **2002**, *92*, 4031–4036. [CrossRef]
96. Lopez, R.; Haynes, T.E.; Boatner, L.A.; Feldman, L.C.; Haglund, R.F., Jr. Temperature-controlled surface plasmon resonance in VO_2 nanorods. *Opt. Lett.* **2002**, *27*, 1327–1329. [CrossRef] [PubMed]
97. Gentle, A.; Maaroof, A.I.; Smith, G.B. Nanograin VO_2 in the metal phase: A plasmonic system with falling resistivity as temperature rises. *Nanotechnology* **2007**, *18*, 025202/1–025202/7. [CrossRef]
98. Bai, H.; Cortie, M.B.; Maaroof, A.I.; Dowd, A.; Kealley, C.; Smith, G.B. The preparation of a plasmonically resonant VO_2 thermochromic pigment. *Nanotechnology* **2009**, *20*, 085607/1–085607/9. [CrossRef] [PubMed]
99. Mlyuka, N.R.; Niklasson, G.A.; Granqvist, C.G. Thermochromic multilayer films of VO_2 and TiO_2 with enhanced transmittance. *Sol. Energy Mater. Sol. Cells* **2009**, *93*, 1685–1687. [CrossRef]
100. Mlyuka, N.R.; Niklasson, G.A.; Granqvist, C.G. Thermochromic VO_2-based multilayer films with enhanced luminous transmittance and solar modulation. *Phys. Status Solidi A* **2009**, *206*, 2155–2160. [CrossRef]
101. Chen, Z.; Gao, Y.; Kang, L.; Du, J.; Zhang, Z.; Luo, H.; Miao, H. VO_2-based double-layered films for smart windows: Optical design, all-solution preparation and improved properties. *Sol. Energy Mater. Sol. Cells* **2011**, *95*, 2677–2684. [CrossRef]
102. Taylor, A.; Parkin, I.; Noor, N.; Tummeltshammer, C.; Brown, M.S.; Papakonstantinou, I. A bioinspired solution for spectrally selective thermochromic VO_2 coated intelligent glazing. *Opt. Expr.* **2013**, *21*, A750–A764. [CrossRef] [PubMed]
103. Zhu, J.; Huang, A.; Ma, H.; Ma, Y.; Tong, K.; Ji, S.; Bao, S.; Cao, X.; Jin, P. Composite film of vanadium dioxide nanoparticles and ionic liquid–nickel–chlorine complexes with excellent visible thermochromic performance. *ACS Appl. Mater. Interfaces* **2016**, *8*, 29742–29748. [CrossRef] [PubMed]
104. Ke, Y.; Balin, I.; Wang, N.; Lu, Q.; Tok, A.I.Y.; White, T.J.; Magdassi, S.; Abdulhalim, I.; Long, Y. Two-dimensional SiO_2/VO_2 photonic crystals with statically visible and dynamically infrared modulated for smart window deployment. *ACS Appl. Mater. Interfaces* **2016**, *8*, 33112–33120. [CrossRef] [PubMed]
105. Ji, Y.-X.; Li, S.-Y.; Niklasson, G.A.; Granqvist, C.G. Durability of thermochromic VO_2 thin films under heating and humidity: Effect of Al oxide top coatings. *Thin Solid Films* **2014**, *562*, 568–573. [CrossRef]
106. Talledo, A.; Granqvist, C.G. Electrochromic vanadium-pentoxide-based films: Structural, electrochemical, and optical properties. *J. Appl. Phys.* **1995**, *77*, 4655–4666. [CrossRef]
107. Lykissa, I.; Li, S.-Y.; Ramzan, M.; Chakraborty, S.; Ahuja, R.; Granqvist, C.G.; Niklasson, G.A. Electronic density-of-states of amorphous vanadium pentoxide films: Electrochemical data and density functional theory calculations. *J. Appl. Phys.* **2014**, *115*, 183701/1–183701/5. [CrossRef]
108. Vernardou, D.; Louloudakis, D.; Spanakis, E.; Katsarakis, N.; Koudoumas, E. Thermochromic amorphous VO_2 coatings grown by APCVD using a single-precursor. *Sol. Energy Mater. Sol. Cells* **2014**, *128*, 36–40. [CrossRef]
109. Ji, Y.-X.; Niklasson, G.A.; Granqvist, C.G. Durability of VO_2-based thin films at elevated temperature: Towards thermochromic fenestration. *J. Phys. Conf. Proc.* **2014**, *559*, 012005. [CrossRef]
110. Tong, K.; Li, R.; Zhu, J.; Yao, H.; Zhou, H.; Zeng, X.; Ji, S.; Jin, P. Preparation of VO_2/Al-O core–shell structure with enhanced weathering resistance for smart window. *Ceram. Int.* **2016**. [CrossRef]
111. Nečas, D.; Klapetek, P. Gwyddion: An open-source software for SPM data analysis. *Cent. Eur. J. Phys.* **2012**, *10*, 181–188. [CrossRef]
112. Grenfell, T.C.; Warren, S.G. Representation of a nonspherical ice particle by a collection of independent spheres for scattering and absorption of radiation. *J. Geophys. Res.* **1999**, *104*, 31697–31709. [CrossRef]
113. Bohren, C.F.; Huffman, D.R. *Absorption and Light Scattering by Small Particles*; Wiley: New York, NY, USA, 1983.
114. Li, S.; Li, Y.; Qian, K.; Ji, S.; Luo, H.; Gao, Y.; Jin, P. Functional fiber mats with tunable diffuse reflectance composed of electrospun VO_2/PVP composite fibers. *ACS Appl. Mater. Interfaces* **2014**, *6*, 9–13. [CrossRef] [PubMed]
115. Qian, K.; Li, S.; Ji, S.; Li, W.; Li, Y.; Chen, R.; Jin, P. Fabrication of VO_2 nanorods/PVP composite fiber mats and their unique optical diffuse reflectance properties. *Ceram. Int.* **2014**, *40*, 14517–14521. [CrossRef]
116. Moot, T.; Palin, C.; Mitran, S.; Cahoon, J.F.; Lopez, R. Designing plasmon-enhanced thermochromic films using a vanadium dioxide nanoparticle elastomeric composite. *Adv. Opt. Mater.* **2016**, *4*, 578–583. [CrossRef]
117. Seeboth, A.; Lötzsch, D. *Thermochromic and Thermotropic Materials*; Pan Stanford Publishing: Singapore, 2014.

118. Anderson, A.D.; Broekhuis, M.D.; Byker, H.J.; DeJong, S.J. Color Neutral Thermochromic Layers and Laminates. U.S. Patent No. 9,465,239, 11 October 2016.
119. Jelle, B.P.; Hynd, A.; Gustavsen, A.; Arasteh, D.; Goudey, H.; Hart, R. Fenestration today and tomorrow: A state-of-the-art review and future research oppoprtunities. *Sol. Energy Mater. Sol. Cells* **2012**, *96*, 1–28. [CrossRef]
120. Niklasson, G.A.; Granqvist, C.G. Electrochromics for smart windows: Thin films of tungsten oxide and nickel oxide, and devices based on these. *J. Mater. Chem.* **2007**, *17*, 127–156. [CrossRef]
121. Granqvist, C.G. Electrochromics for smart windows: Oxide-based thin films and devices. *Thin Solid Films* **2014**, *564*, 1–38. [CrossRef]
122. Mortimer, R.J.; Rosseinsky, D.R.; Monk, P.M.S. *Electrochromic Materials and Devices*; Wiley-VCH: Weinberg, Germany, 2015.
123. Powell, M.J.; Quesada-Cabrera, R.; Taylor, A.; Teixeira, D.; Papakostantinou, I.; Palgrave, R.G.; Sankar, G.; Parkin, I.P. Intelligent multifunctional $VO_2/SiO_2/TiO_2$ coatings for self-cleaning, energy-saving window panels. *Chem. Mater.* **2016**, *28*, 1369–1376. [CrossRef]